Journal of Solid State Chemistry **142,** 360–367 (1999)
Article ID jssc.1998.8044, available online at http://www.idealibrary.com on IDEAL®

Crystal Structure of α-$AgVO_3$ and Phase Relation of $AgVO_3$

Shigeharu Kittaka,[1] Kosaku Matsuno, and Haruo Akashi*

*Department of Chemistry, Faculty of Science, and *Research Institute of Natural Sciences, Okayama University of Science, 1-1 Ridaicho, Okayama 700-0005, Japan*

Received June 4, 1998; in revised form September 17, 1998; accepted September 21, 1998

Phase relations of $AgVO_3$ were studied by crystal structure analysis and thermal property measurement. Crystal structure of newly defined α-$AgVO_3$ was determined by XRD measurements. The structure analyzed is monoclinic [$C2/c(\#15)$] and the crystal parameters are $a = 10.437$ Å, $b = 9.897$ Å, $c = 5.532$ Å, and $\beta = 99.69°$, α-$AgVO_3$ is a metastable phase which can be formed by precipitation at an ambient temperature and/or when it is quenched from its melted state. It is also formed just below the melting point instantaneously when cooled slowly and frozen quickly. α-$AgVO_3$ is irreversibly transformed into β-$AgVO_3$ at around 200°C. The β-phase is molten at 476°C. © 1999 Academic Press

INTRODUCTION

A number of silver vanadates, which vary in Ag, V, and O contents, have been studied since the 1960s (1–4). However, there are many substances among this system whose crystal structures have not been confirmed and thus more efforts are required to clarify these (5–8). $AgVO_3$ is one of them. However, this has scarcely been studied in morphologies after the work by Fleury and Kohlmuller in 1966 (4). They proposed three modifications, α-, β-, and γ-types by presenting the XRD results without structural analyses. Since then, research on the α- and γ-type samples has been nil in any form, while some reports can be found on the structure of β-$AgVO_3$ (7, 8). We can precipitate the $AgVO_3$ by reacting Ag^+ and VO_3^-, which gives a well defined powder XRD pattern. This phase is assigned as a composite oxide of α- and γ-type $AgVO_3$ according to the Fleury and Kohlmuller definition. Recently, we were able to form needle-like particles by mixing V_2O_5 sol and $AgNO_3$ solution, which might result in a single crystal but gave an XRD pattern similar to that of the precipitated $AgVO_3$. Besides this confusing fact, a serious deficit for this system is that the crystal structures of these materials have not been confirmed.

[1] To whom correspondence should be addressed. Fax: 086 254 2891: E-mail: kittaka@chem.ous.ac.jp.

In the present paper, phase relations of $AgVO_3$ were studied by crystal structure analysis and thermodynamic measurement. The crystal structure of the low temperature phase (α-$AgVO_3$) was determined.

EXPERIMENTAL

Materials

Three kinds of $AgVO_3$ samples were prepared by employing the three different methods. (i) Sample-1 (S-1) was formed by the precipitation reaction between aqueous $AgNO_3$ (0.1 mol dm^{-3}) and NH_4VO_3 (0.1 mol dm^{-3}), followed by washing with distilled water and drying in air. (ii) S-2 is a needle-like single crystalline particle (Fig. 1). The crystal was grown by aging the precipitate which had been formed by reacting vanadium oxide hydrate $V_2O_5 \cdot nH_2O$ sol (0.2 mol$_{(V)}$ dm^{-3}) with $AgNO_3$ (0.1 mol dm^{-3}) for about 1 year. $V_2O_5 \cdot nH_2O$ sol was prepared by ion-exchange polymerization reaction of recrystallized NH_4VO_3 (9). (iii) S-3 was formed by heating mixture of equivalent amounts of Ag_2O and V_2O_5 at 600°C in air for 1 h, followed by quenching in an ice-water mixture. The XRD patterns of samples S-1 and S-2 are shown by curves 1 and 2 in Fig. 2, respectively. Both patterns coincide completely with each other in the diffraction angles, although intensity relations differ due to the variation of the sample textures. The pattern for S-3 was similar to that for S-1 (not shown). Heat treatment of the sample was conducted in air for 1 h after elevating the temperature and the cooling process was varied to analyze the phase relations. Atomic compositions of the solids were determined by using EPMA (JEOL JXA-8900R).

Crystal Structure Analyses

Crystal structures of powder samples were analyzed by powder XRD (Rigaku RAD-2R: Cu$K\alpha$) single crystal particles were analyzed by use of 4 circle XRD. A needle-like $AgVO_3$ specimen (S-2) having approximate dimensions of

0022-4596/99 $30.00

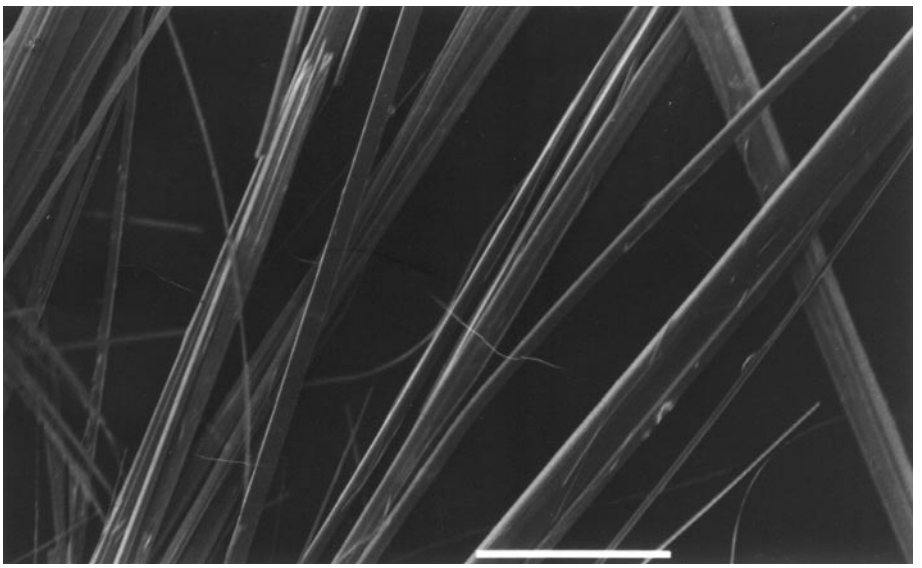

FIG. 1. Scanning electron micrograph of the sample S-2 (α-$AgVO_3$). Bar, 50 μm.

$0.30 \times 0.02 \times 0.01\ mm^3$ was mounted on a glass fiber. The apparatus used was an MXC 18 diffractometer (MAC Science Co.) with graphite monochromated Mo$K\alpha$ radiation. Unit cell constants were obtained from a least-squares fit to the settings for 22 reflections ($20.0 < 2\theta < 35.0^\circ$). Experimental details are listed in Table 1. An empirical absorption correction using the program DIFABS (10) was applied, which gave the transmission factors ranging between 0.85 and 1.00. The data were corrected for Lorentz and polarization effects. Neutral atomic scattering factors were taken from Cromer and Waber (11). Anomalous dispersion effects were included in F_{calc} (12); the values for $\Delta f'$ and $\Delta f''$ were those given by Creagh and McAuley (13). The values for the mass attenuation coefficients are taken from Creagh and Hubbel (14). All the calculations were performed by using the teXsan (15)

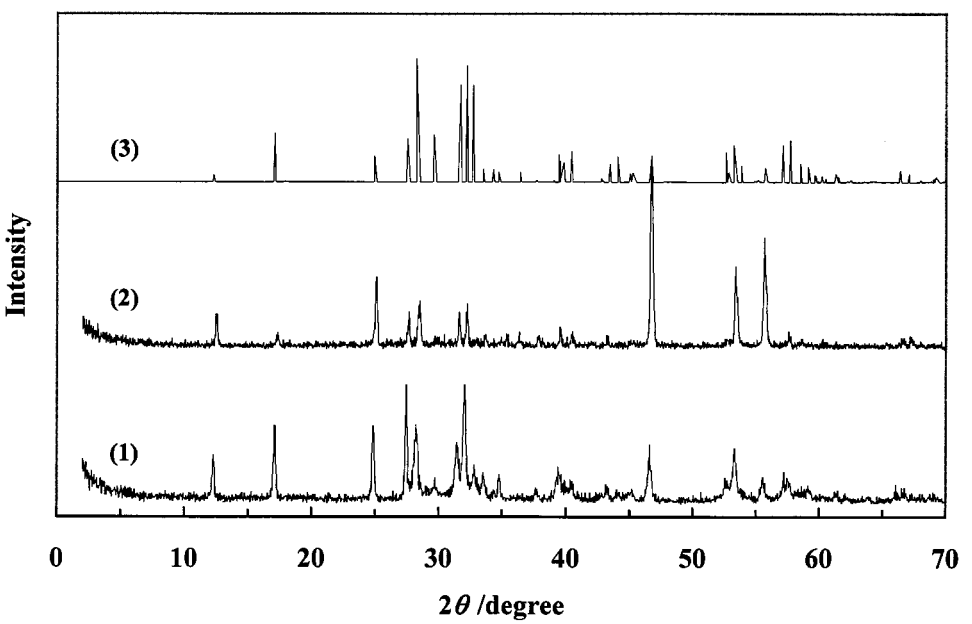

FIG. 2. Powder XRD patterns for the (1) S-1, (2) S-2, and (3) model structure of the α-$AgVO_3$ proposed in the present study.

TABLE 1
Experimental Details and the Parameters Determined
Crystal Data

Empirical formula	$AgVO_3$
Formula weight	206.81
Crystal color	Pale yellow
Crystal dimensions	$0.30 \times 0.02 \times 0.01$ mm^3
Crystal system	Monoclinic
Lattice type	C-centered
No. of reflections used for unit cell determination (2θ range)	22(20.0–35.0°)
Lattice parameters	$a = 10.437(2)$ Å
	$b = 9.897(2)$ Å
	$c = 5.532(4)$ Å
	$\beta = 99.69(4)°$
	$V = 563.3(3)$ Å^3
Space group	$C2/c$ (No. 15)
Z value	8
d_{calc}	4.8761 g/cm^3
F_{000}	752.00
μ(Mo$K\alpha$)	50.01 cm^{-1}
Intensity measurements	
Diffractometer	MXC 18 (MAC Science Co.)
Radiation	Mo$K\alpha$ ($\lambda = 0.71069$ Å) graphite monochromated
Temperature	23.0°C
Scan type	ω
Scan rate	8.0°/min (in ω)
Scan width	$(1.25 + 0.35 \tan\theta)°$
$2\theta_{max}$	55.0°
No. of reflections measured	Total, 756, Unique, 689 ($R_{int} = 0.022$)
Structure solution and refinement	
Structure solution	Direct methods (SHELXS86)
Refinement	Full-matrix least-squares
Function minimized	$\sum w(\|F_o\| - \|F_c\|)^2$
Least squares weights	$w = 1/[\sigma^2(F_o)]$ $= [\sigma_c^2(F_o) + p^2F_o^2/4]^{-1}$
p-factor	0.1003
Anomalous dispersion	All nonhydrogen atoms
No. observations ($I > 3.00\sigma(I)$)	590
No. variables	47
Reflection/parameter ratio	12.55
Residuals: R; R_w	0.033; 0.041
Goodness of fit indicator	0.73
Max shift/error in final cycle	0.00
Maximum (minimum) peak in final diff. map	0.76(− 2.94)e$^-$/Å^3

crystallographic software package of the Molecular Structure Corporation.

Thermal Analysis of $AgVO_3$

Thermal properties were studied by use of DTA (ULVAC TGD-7000). The heating rate was fixed at 5°C min^{-1} and the cooling rate was varied for phase change analyses. All the measurements were conducted in air; since we did not find a significant difference from the measurements in O_2.

Density of $AgVO_3$

In order to confirm the crystal structure of analyzed $AgVO_3$, its density was determined by use of pycnometer (1 cm^3). Water was used as the coexisting liquid.

RESULTS AND DISCUSSION

Phase Relation of $AgVO_3$

Figure 3 shows the DTA curves for samples S-1 and S-2 which have been determined at both ascending and descending directions of temperature. It is seen on curves 1 and 7 that sequential broad endo- and exothermic peaks,

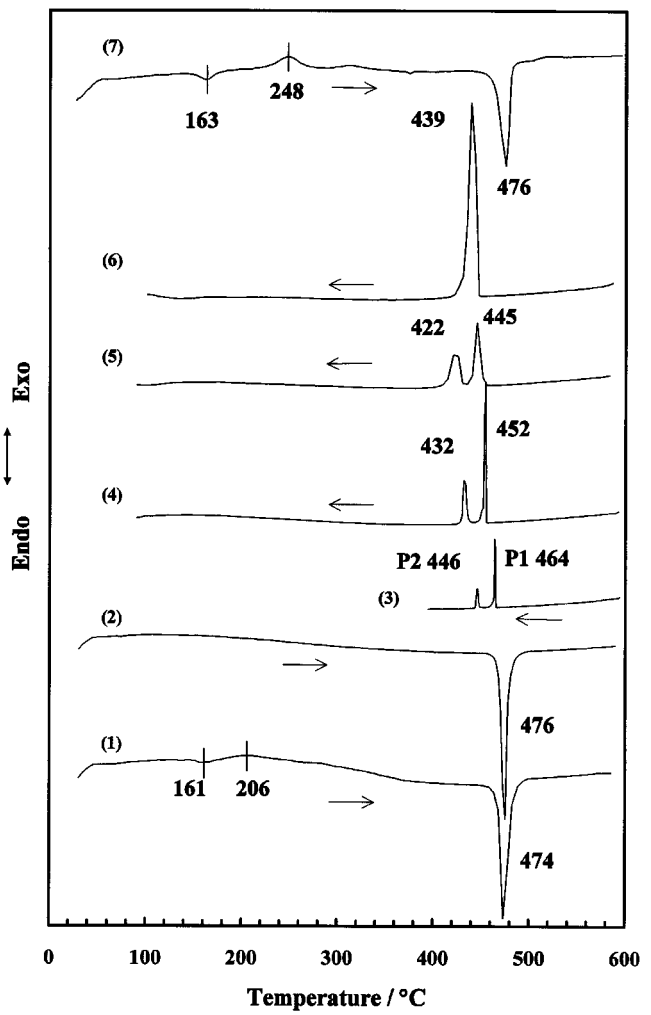

FIG. 3. DTA curves of the precipitate (S-1) and needle-like solid (S-2). Rates of the temperature change (°C min^{-1}) for S-1: elevating direction (1) 5; (2) second run after the (1); descending direction (3) 0.5; (4) 2; (5) 5; (6) 8. S-2: (7) elevating direction at 5 °C min^{-1}.

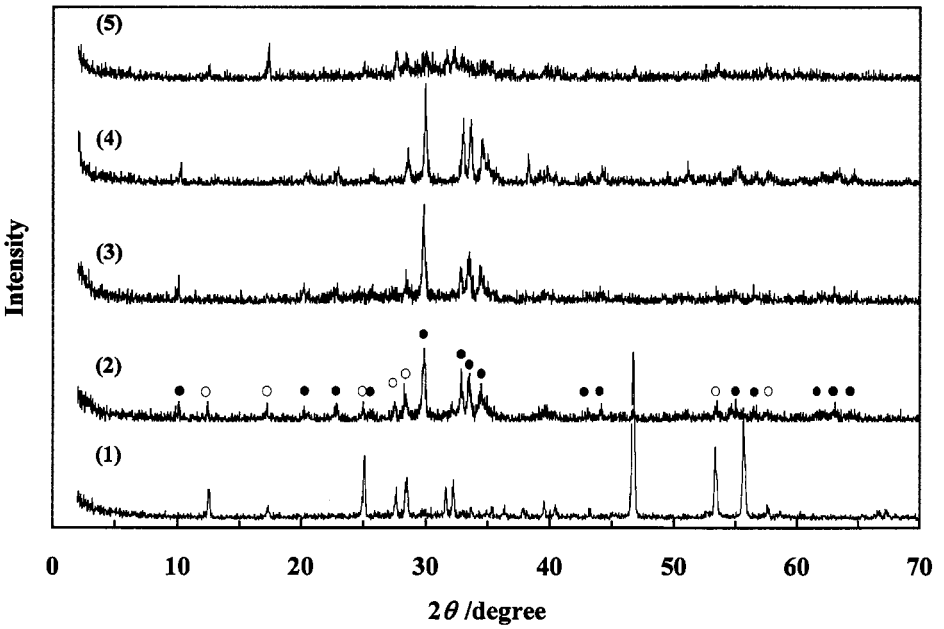

FIG. 4. Powder XRD patterns of $AgVO_3$ (S-2) heated at increasing temperatures and quenched in an ice-water mixture. Heating temperatures (°C): (1) 25 (α); (2) 200 ($\alpha + \beta$); (3) 250 (β); (4) 450 (β); (5) 550 (α). The symbols given after temperatures indicate the crystal structure types: ○, α-$AgVO_3$, ● for β-$AgVO_3$.

which were followed by rather sharp endo-thermic peaks, appeared in both samples: at 161, 206, and 474°C for S-1 and at 163, 248, and 476°C for S-2. The first endothermic peak for both samples cannot be simply assigned to dehydration from the sample, since this is not weakened after evacuation at 50°C. The structure change was not observed either. This requires detailed future research. The second exothermic peak is due to the phase change of the material and will be discussed below. The last endothermic peak was confirmed to be due to melting of the samples. It should be noted that there has not been observed any peak just below the melting point when the temperature is increased. A second run after cooling the molten sample gave simply one endothermic peak at 476°C (curve 2). The sample S-3 provided a curve similar to this.

The XRD measurements were conducted on the heated samples in parallel with DTA measurements. The sample studied was quenched in an ice-water mixture after each heat treatment. Quite similar sequential changes were observed for both samples S-1 and S-2. Representatively, the data for S-2 are shown in Fig. 4. When the sample is heated at 200°C the β-$AgVO_3$ phase appears in addition to the low temperature phase (α- and γ-$AgVO_3$ according to the definition by Fleury and Köhlmuller (3)), above which the β-$AgVO_3$ phase remains up to 450°C. The above authors have claimed that γ-$AgVO_3$ appears between 422 and 478°C although it is not clear if they have made a Debye–Scherrer spectra measurement *in situ* at this temperature range or at room temperature after quenching. However, we can conclude by combination with the DTA data (Fig. 3) that no phase appears between β-$AgVO_3$ and the melt when the system is heated at increasing temperatures. It is interesting to find that the sample quenched in an ice-water mixture after heating at 550°C gave a pattern corresponding to the low temperature phase (curve 5).

In order to clarify this disagreement, DTA analyses were conducted in the cooling direction (curves 3–6 in Fig. 3). The DTA curve determined at $0.5°C\,min^{-1}$ shows two exothermic peaks at 464 (P1) and 446°C (P2). Both peaks displace to lower temperatures with an increasing cooling rate up to $5°C\,min^{-1}$. However, apparent ratios of the peak areas between P1 and P2 do not change so much: quantitative inaccuracy should be considered with the present measuring DTA apparatus. The latter fact suggests that one sample experiences two phase changes during cooling. This can be evidenced by the experimental results. An XRD pattern determined on the sample which has been cooled down to 450°C at the cooling rate $2°C\,min^{-1}$ and quenched in the ice-water mixture is that of the low-temperature phase, and the sample cooled down to 400°C is β-$AgVO_3$. When the cooling rate is increased to more than $5°C\,min^{-1}$, only a single exothermic peak with a rather wide base has appeared as shown by the curve 6 in Fig. 3. The XRD pattern of the sample cooled down to 400°C at $8°C\,min^{-1}$ and quenched is that of β-$AgVO_3$. Furthermore, a sample cooled down to room temperature at $10°C\,min^{-1}$ showed the XRD pattern for β-$AgVO_3$. These facts indicate that the melt is solidified into the β-$AgVO_3$ at one time when the

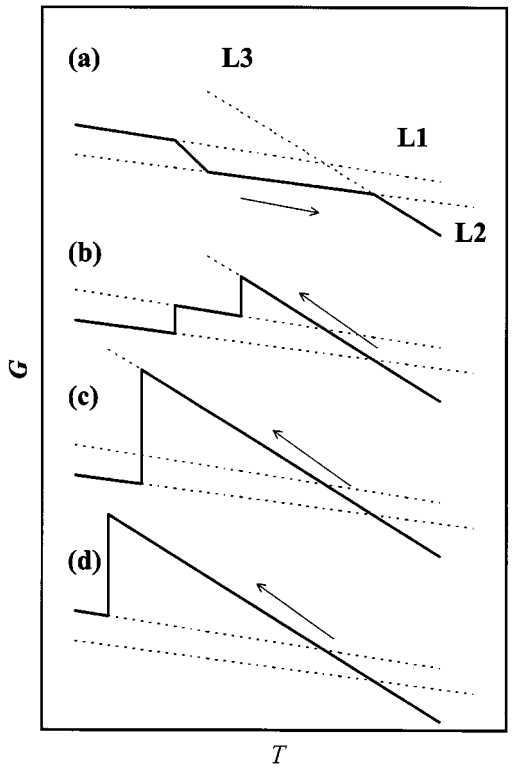

FIG. 5. Illustrations of free energy (G)–temperature (T) relations of $AgVO_3$ and the traces of free energy changes upon thermal treatments. (a) Heating; cooling at (b) slow rate, (c) fast rate; (d) quenched. Line L1 corresponds to α-$AgVO_3$; L2, β-$AgVO_3$; L3, liquid $AgVO_3$.

sample is cooled fast. However, it is to be noted again that melt is solidified to give a low temperature phase when quenched in the ice-water mixture.

The above discussions allowed us to draw the illustrative free energy-temperature diagram illustrated in Fig. 5. (a) In the heating process, the free energy of low temperature phase decreases on Line L1 and drops down to Line L2 for β-$AgVO_3$ over a rather wide temperature region ($\sim 200^\circ$C), by which broad exothermic heat is observed. When the temperature is increased further, the free energy of the system crosses Line L3 and the substance melts by absorbing heat. (b) When the molten $AgVO_3$ is cooled down at the moderate speed, the free energy of the system increases on line L3 up to above L1 (i.e., the system is supercooled) and drops at some temperature on the L1 system, accompanied by crystallization of the low-temperature phase. This step gives the first exothermic peak P1 (curves 3–5 in Fig. 3). (c) Upon further cooling, the free energy increases for a while on line L1 and again drops down onto line L2 for β-$AgVO_3$, ejecting the heat for the transition P2. (d) When

TABLE 2
Atomic Coordinates, B_{eq}, and Wyckoff Letters

Atom	x	y	z	B_{eq}	Wyckoff letter
Ag(1)	0.0000	0.58892(4)	0.2500	1.54(1)	e
Ag(2)	0.0000	0.21547(5)	0.2500	1.43(1)	e
V(1)	0.30067(7)	0.41408(6)	0.2150(1)	0.80(2)	f
O(1)	0.1394(4)	0.4040(3)	0.1715(8)	1.60(8)	f
O(2)	−0.1355(4)	0.7722(4)	0.3312(7)	1.81(7)	f
O(3)	0.3533(3)	0.5499(3)	0.4265(5)	1.24(6)	f

Note. $B_{eq} = 8/3\pi^2(U_{11}(aa^*)^2 + U_{22}(bb^*)^2 + U_{33}(cc^*)^2 + 2U_{12}(aa^*bb^*)\cos\gamma + 2U_{13}(aa^*cc^*)\cos\beta + 2U_{23}(bb^*cc^*)\cos\alpha)$.

TABLE 3
Anisotropic Displacement Parameters

Atom	U_{11}	U_{22}	U_{33}	U_{12}	U_{13}	U_{23}
Ag(1)	0.0168(3)	0.0145(3)	0.0255(3)	0.0000	−0.0016(2)	0.0000
Ag(2)	0.0171(3)	0.0167(3)	0.0203(3)	0.0000	0.0028(2)	0.0000
V(1)	0.0096(4)	0.0120(4)	0.0090(4)	0.0006(2)	0.0020(3)	0.0009(2)
O(1)	0.012(2)	0.023(2)	0.025(2)	0.000(1)	0.004(1)	−0.001(1)
O(2)	0.025(2)	0.021(2)	0.023(2)	0.008(1)	0.005(1)	0.007(1)
O(3)	0.018(1)	0.020(2)	0.010(1)	−0.003(1)	0.004(1)	−0.004(1)

Note. The general temperature factor expression: $\exp(-2\pi^2(a^{*2}U_{11}h^2 + b^{*2}U_{22}k^2 + c^{*2}U_{33}l^2 + 2a^*b^*U_{12}hk + 2a^*c^*U_{13}hl + 2b^*c^*U_{23}kl))$.

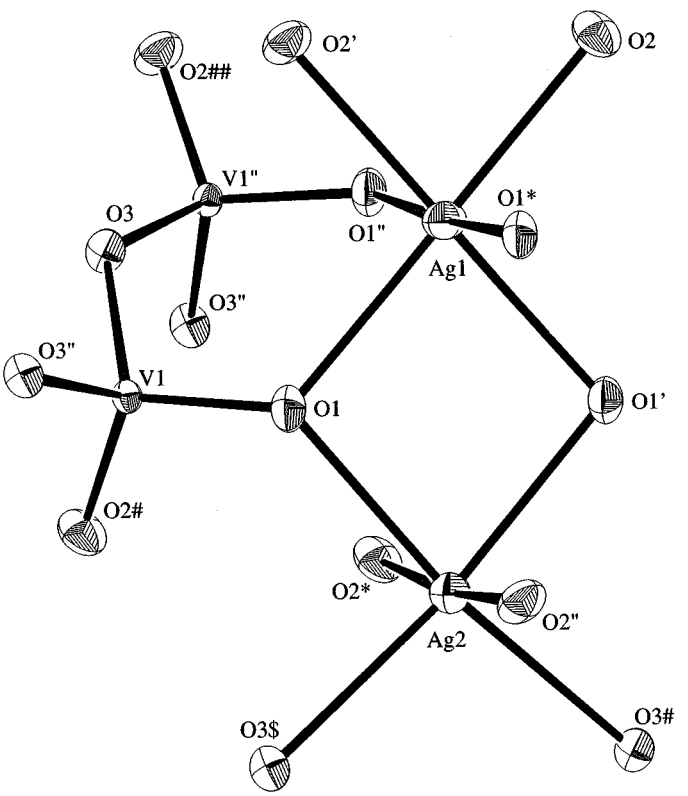

FIG. 6. Ortep image of an α-$AgVO_3$ cluster.

TABLE 4
Interatomic Distance for α-$AgVO_3$

Atoms	Distance/Å	Atoms	Distance/Å
Ag(1) O(1)	2.422(3)	Ag(2) O(3#)	2.547(3)
Ag(1) O(1*)	2.533(4)	V(1) O(1)	1.663(3)
Ag(1) O(2)	2.389(3)	V(1) O(3)	1.806(3)
Ag(2) O(1)	2.450(3)	V(1) O(3″)	1.809(3)
Ag(2) O(2*)	2.506(4)		

Note. Symmetry operators: ′, $-x, +y, \frac{1}{2}-z$; *, $-x, 1-y, -z$; ″, $+x, 1-y, \frac{1}{2}+z$; #, $x-\frac{1}{2}, y-\frac{1}{2}, +z$; $, $\frac{1}{2}-x, y-\frac{1}{2}, \frac{1}{2}-z$.

TABLE 5
Density of α-$AgVO_3$ and β-$AgVO_3$

α-$AgVO_3$ (g cm^{-3})		β-$AgVO_3$ (g cm^{-3})	
Calculated	4.876	Calculated (7)	5.438
S1	4.80	S1 heated at 350°C	5.39
S2	4.82	—	—
Quenched after melting S1	4.81	Cooled slowly after melting S1	5.32

the melt is quenched in the ice-water mixture, it is solidified as a low-temperature phase along the G–T line dropping on Line L1.

Crystal Structure of $AgVO_3$ Stable at Low Temperatures

Although above phase relations must be confirmed through more detailed techniques, the most important thing to be clarified now seems to be the crystal structure of the low-temperature phase of $AgVO_3$. We could grow a needle-like crystal S-2 whose XRD pattern is the same as that of S-1 (Fig. 2) and come to believe that the low-temperature material is a single phase different from that assigned by Fleury and Köhlmuller (7) and conduct the crystal structure analysis through XRD.

As Table 1 shows, the analyzed result of the crystal structure may be reliable with the small values of R (0.033) and R_w (0.041). The detailed atomic coordinates in the unit cell were described in Table 2 together with B_{eq} and

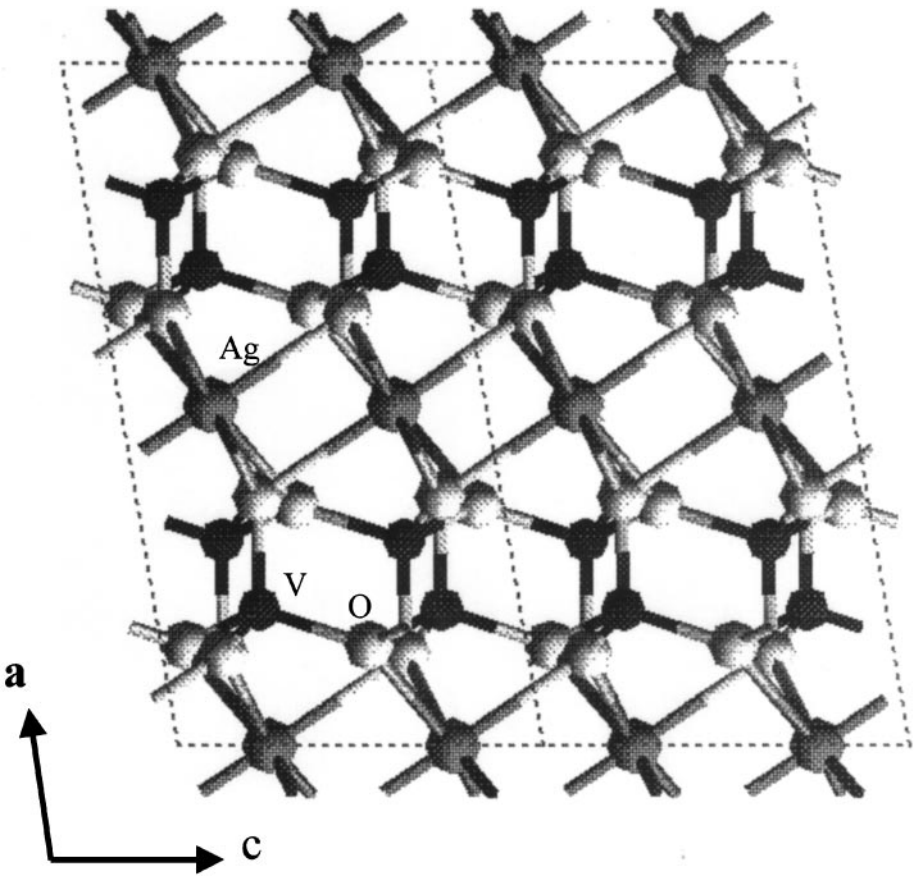

FIG. 7. A sketch of two unit cells of the α-$AgVO_3$ arrayed to the *c*-direction, which is projected along the *b*-axis.

Wyckoff letters. Anisotropic displacement parameters for component atoms were shown in Table 3 and the interatomic bond lengths for the material in Table 4. The simulated powder diffraction pattern from the structure analyzed agrees with the observed diffraction patterns for the samples precipitated (S-1) and needle-like particles (S-2), as shown in Fig. 2. We would like to define this structure as "α-$AgVO_3$." The illustrations of the structure are given by an image of a cluster and a sketch illustrating the coordination image in the unit cell in Figs. 6 and 7, respectively. Table 5 shows the densities of α-$AgVO_3$ experimentally determined (4.81 $g\,cm^{-3}$) and calculated on the simulated structure (4.876 $g\,cm^{-3}$). Both values are quite close with each other which substantiates the validity of the present simulation of the structure.

These results indicate the large difference of the bonding modes of both Ag and V from those of β-$AgVO_3$ on the following points (7). Only one kind of V site is present in the α-$AgVO_3$: an almost regular tetrahedron was formed with O. This is in contrast to the four kinds of distorted octahedraly coordinated ones for the β-$AgVO_3$ and sounds exceptional among vanadium ions in the variety of vanadium oxide bronzes: octahedral and pyramidal coordination is common (16, 17). It is interesting also to find the zigzag chain formation between VO_4 tetrahedrons by sharing the corner O along the *c*-axis as shown in Fig. 7.

Two kinds of Ag ion sites, which are coordinated by distorted octahedrons of O ions, are shown in Fig. 6. These coordination modes of Ag gave the arrangements of octahedrons expanding to the *c*-direction by sharing the edges as shown in Fig. 7. Between the two neighboring octahedron sheets (in the center of the cell in Fig. 8) we can see a channel which runs in the *c* direction. The zigzag chains of tetrahedrons of VO_4 which are sandwiched between the sheets of octahedrons form the smaller atomic packing compared with the octahedrons as found in many vanadate bronzes, especially with the β-$AgVO_3$ (5.32 $g\,cm^{-3}$) in which polyhedrons formed by O ions are occupied by metal ions (7). The fact that the α-$AgVO_3$ phase is solidified just below the melting point rather than the β-$AgVO_3$ phase seems to be related to this lower density of the former phase. That is, the local structure of the molten phase should be similar to that of α-$AgVO_3$ and it will be easy to freeze this structure at the temperature just below the melting point. The similar phenomenon that the low density phase is quenched easily from the melt have been observed in TiO_2 and Al_2O_3 by the present authors (18, 19). It is anticipated that the cooling at the smallest rate employed here in Fig. 3

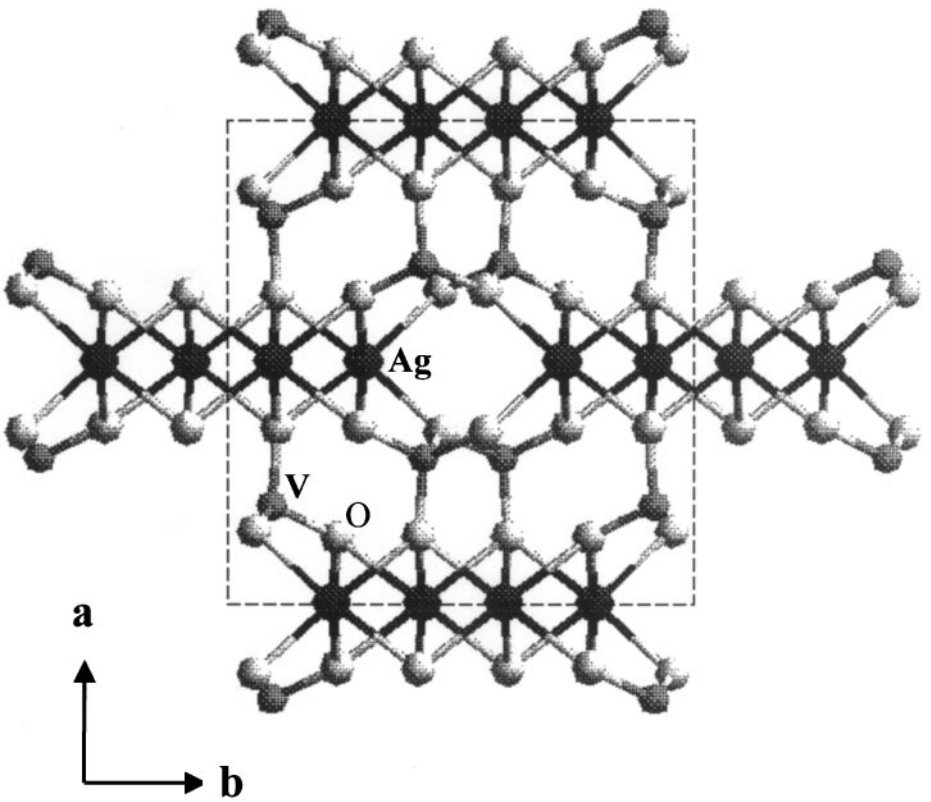

FIG. 8. A sketch of the unit cell of α-$AgVO_3$ which is projected along the *c*-axis.

(3) is still too fast to conduct the solidification tracing the lowest free energy line of Fig. 5.

CONCLUSIONS

The determination of the crystal structure of the low temperature phase, α-$AgVO_3$, clarified the phase properties of the $AgVO_3$ system. $AgVO_3$ is composed of two morphologies, metastable α-$AgVO_3$ and stable β-$AgVO_3$. The α-$AgVO_3$ is formed by a sedimentation reaction of aqueous Ag^+ with VO_3^- or by quenching of the melt. The very low density of the material explains the quenchiability of the α-phase from the liquid. β-$AgVO_3$ is formed by heating the former to around 200°C and cooling slowly from the melt.

ACKNOWLEDGMENTS

The authors express sincere thanks to Dr. Genta Sakane for his assistance in crystal structure analysis and to Professor Hirotsugu Nishido for the chemical analyses of the products by EPMA measurements. Financial support, Special Grant for Cooperative Research administered by the Japan Private School Promotion Foundation, and Grant-in-Aid for Exploratory Research 09874148, are also thanked.

REFERENCES

1. P. Hagenmuller, J. Galy, M. Pouchard, and A. Casalot, *Mater. Res. Bull.* **1,** 45 (1966).
2. B. Raveau, *Rev. Chim. Miner.* **4,** 729–58 (1967).
3. A. Casalot and M. Pouchard, *Bull. Soc. Chim. Fr.* 3817 (1967).
4. P. Fleury and R. Köhlmuller, *Compt Rend. Acad. Sci. Paris* **262,** 475 (1966).
5. M. Ha-Eierdanz and U. Müller, *Z. Anogr. Allg. Chem.* **619,** 287 (1993).
6. H. W. Zandbergen, A. M. Crespi, P. M. Skarstad, and J. F. Vente, *J. Solid State Chem.* **110,** 167 (1994).
7. P. Rozier, J. M. Savariault, and J. Galy, *J. Solid State Chem.* **122,** 303 (1996).
8. S. Hayakawa, T. Yoko, and S. Sakka, *J. Solid State Chem.* **112,** 329 (1994).
9. S. Kittaka, Y. Ayatsuka, K. Ohtani, and N. Uchida, *J. Chem. Soc. Faraday Trans.* I **85,** 3825 (1989).
10. N. Walker and N. Stuart, *Acta Crystallogr. A* **39,** 158 (1983).
11. D. T. Cromer, and J. T. Waber, "International Tables for X-ray Crystallography," Vol. IV, Table 2.2 A. Kenosha Press, Birmingham, England, 1974.
12. J. A. Ibers and W. C. Hamilton, *Acta Crystallogr.* **17,** 781 (1964).
13. D. C. Creagh and W. J. McAuley, *in* "International Tables for Crystallography" (A. J. C. Wilson, Ed.), Vol. C, p. 219, Table 4.2.6.8. Kluwer Academic, Boston, 1992.
14. D. C. Creagh and J. H. Hubbell, *in* "International Tables for Crystallography" (A. J. C. Wilson, Ed.), Vol. C, p. 200, Table 4.2.4.3. Kluwer Academic, Boston, 1992.
15. "Crystal Structure Analysis Package." Molecular Structure Corporation, 1985, 1992.
16. J. Galy, *J. Solid State Chem.* **100,** 229 (1992).
17. C. N. R. Rao and B. Raveau, "Transition Metal Oxides," VCH, New York, 1995.
18. T. Morimoto and S. Kittaka, *J. Colloid Interface Sci.* **78,** 356 (1980).
19. S. Kittaka and T. Morimoto, *Bull. Chem. Soc. Jpn.* **54,** 2882 (1981).